Session 1P2
Electromagnetic Modeling in Optoelectronics

Simulation of Self-assembled Photonic Crystals with Embedded Waveguide Using FDTD Method

J.-U. Lee[1], **K.-H. Baek**[1], **C. Olson**[1], **D. M. Kim**[1,2], **and A. Gopinath**[1]

[1]University of Minnesota, USA
[2]Kookmin University, Korea

Photonic crystals (PCs) with three-dimensionally periodic structures and omnidirectional photonic bandgaps (PBGs) within certain wavelength ranges have attracted extensive interest in their various potential applications in integrated photonics and optics. Artificial planar, line, or point defects embedded in the PCs, which allow propagating or localizing light, are required for the applications. One of the 3-D PBG structures, self-assembled PCs (inverse opals) with embedded defects has been investigated widely due to its simple and low-cost fabrication process. Ordered templates with close-packed face centered cubic structure may be built by the colloidal spheres, and is selectively removed after infiltrating a semiconductor material with high-refractive index into the interstitials of spheres.

A complete numerical characterization of the self-assembled PCs with a defect is essential for guiding the design process and obtaining a deeper insight into the physics of PCs. One of the numerical techniques, the Finite Difference Time Domain (FDTD) method for simulating the interaction of electromagnetic fields with material structures has become a well-established tool for the analysis of PCs. For predicting the PC behaviors and designing proper applications, we need to accurately model the PCs and their applications using the FDTD method.

In this paper, the numerical analysis using FDTD method for 3-D self-assembled inverse opal structures with embedded line defects is discussed. No previous results of such investigation have been reported. To confirm the existence of specific PBGs of self-assembled PCs, we calculated photonic band structures and transmittance spectrum using the MIT Photonic-Bands program based on Plane-Wave method and the Rsoft Fullwave FDTD codes, respectively. The simulation results for the 3-D PCs with close-packed air spheres surrounded by silicon suggest that the air spheres with diameter of 870 nm are required for a PBG at wavelength of 1550 nm, and the band structure of 3-D inverse opal shows an omnidirectional PBG exists. A line defect, Si_3N_4 rectangular channel waveguide embedded in the 3-D self-assembled PCs was used for the propagation simulations of light at wavelength of 1550 nm and the transmission spectrums of the waveguides were measured using the FDTD codes. We confirmed that guided wave propagation occurred along the Si_3N_4 guide within the PBG. Simulation results on both the 2-D and 3-D inverse opals with embedded waveguides will be presented at meeting.

Modal Analysis and Beam Propagation in Bent Fibers

G. R. Hadley
Sandia National Laboratories, USA

After three or four decades, fiber optics is still finding new applications both in communications and more recently in high-power lasers and amplifiers for medicine and materials processing. These new applications often require bending the fiber to ensure single mode operation and therefore maintain a high brightness output. Bent fibers also offer a means for polarization control. In these cases numerical models are needed that accurately handle the radiation loss resulting from the bending while keeping all relevant field components. To this end, we have developed a suite of tools for modeling bent fibers that address these issues. Our numerical models are triangular-grid finite difference based in cylindrical coordinates so that radiation loss is naturally handled as a curvilinear coordinate system effect, rather than by artificially adding on an index ramp as is typically done. Our suite of codes includes both full vector and semivectorial eigenmode solvers and beam propagation codes. These tools have recently been modified to include Kerr effect nonlinearities, and thus both the model derivation and its applications for predicting self-focusing effects in MW fiber amplifiers will be presented.

Hybrid Methods for Efficient Electromagnetic Simulation

T. M. Benson, **P. Sewell**, **A. Vukovic**
C. Christopoulos, **D. W. P. Thomas**, **and A. Nosich**
University of Nottingham, UK

Simulation of the electromagnetic behavior of very general structures is a common activity in many branches of science and technology and many techniques have been proposed and exploited for this purpose. The use of general-purpose time-domain numerical techniques such as the Finite Difference Time Domain (FDTD) [1] and Transmission Line Modeling (TLM) methods [2] is becoming widespread, due to their flexibility and relative ease of use. These techniques offer the flexibility to deal with relatively arbitrary geometries and a wide range of material properties. Unfortunately, the flexibility of numerical simulation tools is often bought at the expense of computational efficiency, both in terms of run times and memory consumption. In particular, their space discretizing nature means that they do not effectively model free-space regions.

Alternative Integral Equation approaches to both frequency and time domain simulations intrinsically incorporate our physical understanding of the relatively simple behavior of electromagnetic fields in uniform spaces [3, 4]. There is no need to terminate the calculation window with artificial absorbers as the kernel of the integral equation intrinsically contains the correct asymptotic behavior at infinity. We will show that such formulations can offer clear computational advantage, especially when the problem space considered contains large uniform regions or the geometry cannot readily be spatially discretized without stair-stepping error.

Having considered these two alternative approaches to electromagnetic simulation we will go on to discuss hybrid simulation techniques, where different simulation tools are used to model those parts of a particular problem to which they are best suited. By embedding a numerical algorithm such as TLM within a global region described by the Integral Equation method, and coupling tools together through a suitable interface, an overall efficiency saving can be achieved [5].

REFERENCES

1. Taflove, A., "Computational electrodynamics: the finite-difference time-domain method," Artech House, Norwood, MA, 1995.
2. Christopoulos, C., "The transmission-line modeling method: TLM," *IEEE Press*, Piscataway, NJ, 1995.
3. Boriskina, S. V. and A. I. Nosich,, "Radiation and absorption losses of the whispering-gallery-mode dielectric resonators excited by a dielectric waveguide," *IEEE Trans. Microwave Theory Tech.*, Vol. 47, 224–231, 1999.
4. Fedotov, F. V., A. G. Nerukh, T. M. Benson, and P. Sewell, "Investigation of electromagnetic field in a layer with time varying medium by volterra integral equation method," *J. Lightwave Technology*, Vol. 21, 305–314, 2003.
5. Lindenmeier, S., L. Pierantoni, and P. Russer, "Hybrid space discretising integral equation methods for numerical modelling of transient interference," *IEEE Trans. on Electromagnetic Compatibility*, Vol. 41, 425–430, 1999.

Applying Oblique Coordinates in the Method of Lines

S. F. Helfert
University of Hagen, Germany

Abstract—Oblique coordinates are introduced into the method of lines. For the purpose of analysis, suitable equations are derived. The formulas are applied to compute the transmission in a waveguide device consisting of straight waveguides connected by a tilted one. Furthermore, the band structure of a hexagonal photonic bandgap structure was computed using these oblique coordinates.

1. Introduction

The Method of Lines (MoL) [1] has been proven as an efficient tool for modeling waveguide structures in the microwave area and in optics. Depending on the structure under study various coordinate systems like Cartesian or cylindrical ones have been introduced, the latter allowing to examine e. g., VCSEL-structures or curved waveguides [2–5]. Formulas for arbitrary rectangular coordinates can be found in [6].

By introducing Floquet's theorem into the MoL [7, 8] photonic crystal structures (PCs) with a square lattice could examined [9, 8]. Due to the shape of these structures Cartesian coordinates were applied.

In contrast, the shape of the elementary cells in hexagonal structures is not rectangular. Motivated by papers found in the literature (e. g., [10–12]) an algorithm was developed that uses oblique coordinates. In the references given above algorithms for the TE-polarization (2D) were described. Here we will derive expressions for the full 3D-vectorial case from which the two-dimensional case can be easily derived.

The formulas were used to compute the propagation characteristic in a waveguide device, where two straight waveguides were connected with a tilted one. The results were compared with those obtained by a staircase approximation showing a very good agreement. As second application the band-structure of PCs with a hexagonal lattice was computed.

2. Theory

In this section we are going to derive the equations that can be used for analyzing devices with oblique coordinates. We will start with Maxwell's equations from which we determine the equations for the full vectorial case. Simpler formulas (i.e., for two-dimensional structures) are then derived from these expressions.

Consider the coordinate system shown in Fig. 1, which shows Cartesian coordinates and oblique ones. The relation between oblique coordinates (u, v, y) and Cartesian ones (x, y, z) is given as:

$$x = u\sin(\theta) + v \tag{1}$$
$$z = u\cos(\theta) \tag{2}$$
$$y = y \tag{3}$$

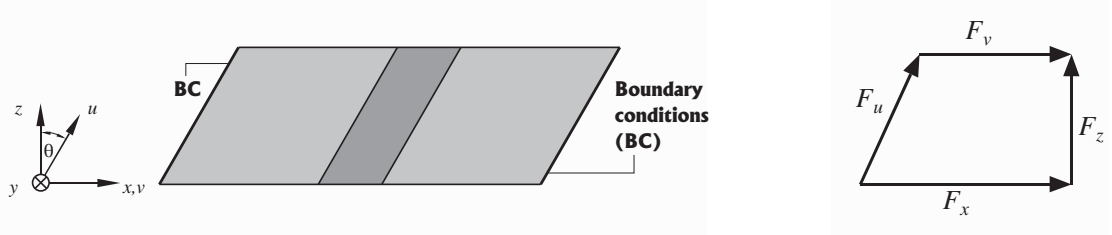

Figure 1: Tilted waveguide structure in an oblique coordinate system, and relation between the field components.

The y-coordinate is identical in both systems. Therefore, in the following, we will examine only the remaining ones. Next, we need the derivatives with respect to the u- and v-coordinate. By inverting the relations in (1)

and (2) and applying the chain rule, we obtain:

$$\frac{\partial}{\partial x} = \frac{\partial}{\partial u}\frac{\partial u}{\partial x} + \frac{\partial}{\partial v}\frac{\partial v}{\partial x} = \frac{\partial}{\partial v} \tag{4}$$

$$\frac{\partial}{\partial z} = \frac{\partial}{\partial u}\frac{\partial u}{\partial z} + \frac{\partial}{\partial v}\frac{\partial v}{\partial z} = \frac{1}{\cos(\theta)}\frac{\partial}{\partial u} - \tan(\theta)\frac{\partial}{\partial v} \tag{5}$$

At interfaces between two waveguide sections the transverse components have to be continuous. These are the x- and the y-component in Cartesian coordinates. A closer look at Fig. 1 shows that the x-component is put together of the u- and v-component if oblique components are used. However, also in an oblique coordinate system we find that the x-component itself is continuous. Therefore, we will use the Cartesian components (i.e., x- and y-component) of the fields in oblique coordinates as well.

To derive suitable equations for these components, we start with Maxwell's equations:

$$\overline{\nabla} \times \vec{H} = j\varepsilon_{\mathrm{r}}\vec{E} \qquad\qquad \overline{\nabla} \times \vec{E} = -j\mu_{\mathrm{r}}\vec{\tilde{H}} \tag{6}$$

where the coordinates have been normalized with the free-space wavenumber k_0, (e. g., $\overline{y} = k_0 y$). Furthermore, the magnetic field was normalized with the free space wave impedance $\eta_0 = 120\pi\,\Omega$: $\vec{\tilde{H}} = \eta_0\vec{H}$. Now, the derivatives with respect to x and z are replaced by those with respect to u and v and the z-component of the electric and magnetic field is substituted by the x- and y-components. This leads to the following first order differential equation system:

$$\frac{1}{\cos(\theta)}\frac{\partial}{\partial \overline{u}}\vec{F} + Q\vec{F} = \vec{0} \qquad \text{with} \qquad \vec{F} = \begin{pmatrix} E_x \\ \widetilde{H}_y \\ E_y \\ \widetilde{H}_x \end{pmatrix} \tag{7}$$

and

$$Q = \begin{bmatrix} -\tan(\theta)\dfrac{\partial}{\partial\overline{v}} & j\left(\mu_{\mathrm{r}} + \dfrac{\partial}{\partial\overline{v}}\dfrac{1}{\varepsilon_{\mathrm{r}}}\dfrac{\partial}{\partial\overline{v}}\right) & 0 & -j\dfrac{\partial}{\partial\overline{v}}\left(\dfrac{1}{\varepsilon_{\mathrm{r}}}\dfrac{\partial}{\partial\overline{y}}\right) \\ j\left(\varepsilon_{\mathrm{r}} + \dfrac{\partial}{\partial\overline{y}}\dfrac{1}{\mu_{\mathrm{r}}}\dfrac{\partial}{\partial\overline{y}}\right) & -\tan(\theta)\dfrac{\partial}{\partial\overline{v}} & -j\dfrac{\partial}{\partial\overline{y}}\left(\dfrac{1}{\mu_{\mathrm{r}}}\dfrac{\partial}{\partial\overline{v}}\right) & 0 \\ 0 & j\dfrac{\partial}{\partial\overline{y}}\left(\dfrac{1}{\varepsilon_{\mathrm{r}}}\dfrac{\partial}{\partial\overline{v}}\right) & -\tan(\theta)\dfrac{\partial}{\partial\overline{v}} & -j\left(\mu_{\mathrm{r}} + \dfrac{\partial}{\partial\overline{y}}\dfrac{1}{\varepsilon_{\mathrm{r}}}\dfrac{\partial}{\partial\overline{y}}\right) \\ j\dfrac{\partial}{\partial\overline{v}}\left(\dfrac{1}{\mu_{\mathrm{r}}}\dfrac{\partial}{\partial\overline{y}}\right) & 0 & -j\left(\varepsilon_{\mathrm{r}} + \dfrac{\partial}{\partial\overline{v}}\dfrac{1}{\mu_{\mathrm{r}}}\dfrac{\partial}{\partial\overline{v}}\right) & -\tan(\theta)\dfrac{\partial}{\partial\overline{v}} \end{bmatrix}$$

To solve this equation, we proceed as usual in the method of lines. We divide the structure under study in sections where the permittivity and the permeability (the latter usually being equal to one) depend only on the transverse coordinates (v, y). Then, the derivatives with respect to v and y are discretized with finite differences. This results in a system of coupled ordinary differential equations:

$$\frac{\partial}{\partial\overline{u}}\mathbf{F} + \overline{\boldsymbol{Q}}\,\mathbf{F} = \mathbf{0} \tag{8}$$

where the operator $\boldsymbol{Q}$ had been multiplied with $\cos(\theta)$: $\cos(\theta)\boldsymbol{Q} = \overline{\boldsymbol{Q}}$. By transformation to the principle axes we can decouple this system

$$\overline{\boldsymbol{Q}} = \boldsymbol{T}\boldsymbol{\Gamma}\boldsymbol{T}^{-1} \qquad\qquad \mathbf{F} = \boldsymbol{T}\,\overline{\mathbf{F}}$$

with the solution

$$\overline{\mathbf{F}}(\overline{u}) = \exp(-\boldsymbol{\Gamma}\overline{u})\,\overline{\mathbf{F}}(0) \tag{9}$$

The eigenvectors of $\overline{\boldsymbol{Q}}$ give the electric and magnetic field distribution of the eigenmodes and the eigenvalues $\boldsymbol{\Gamma}$ are the corresponding propagation constants. Since we are dealing with a first order differential equation system here, the forward and the backward propagating modes are determined at the same time. Therefore, we can divide the eigenvalues/eigenvectors according to

$$\boldsymbol{\Gamma} = \mathrm{diag}(\boldsymbol{\Gamma}_\mathrm{f}, -\boldsymbol{\Gamma}_\mathrm{b}) \qquad \text{with} \qquad \mathrm{Re}(\boldsymbol{\Gamma}_\mathrm{f}, \boldsymbol{\Gamma}_\mathrm{b}) > 0 \qquad \text{and} \qquad \boldsymbol{T} = \begin{bmatrix} \boldsymbol{T}_\mathrm{Ef} & \boldsymbol{T}_\mathrm{Eb} \\ \boldsymbol{T}_\mathrm{Hf} & \boldsymbol{T}_\mathrm{Hb} \end{bmatrix}$$

Now, the next steps of analyzing complex circuits with the MoL are analogous to those in Cartesian coordinates. Therefore, we give just a short summary here. After having found the solution in the homogeneous sections, we have to consider the continuity at the interfaces. Together with boundary conditions at the input and the output of the device, we could e. g., derive transfer matrix formulas for the whole structure. However, these transfer matrix expressions are potentially unstable, because of the exponentially increasing terms. Therefore, we use scattering parameters or alternatively impedances/admittances. In both of these cases, we start at the output of our structure. When using scattering parameters we define a reflection coefficient as the ratio between the backward and the forward propagation modes:

$$\mathbf{F}_\mathrm{b} = \overline{\boldsymbol{r}}\ \mathbf{F}_\mathrm{f}$$

This reflection coefficient is transformed to the input of the device. We have to consider homogeneous sections and the interfaces between these sections. In a homogeneous section with the length d, we obtain for the transformation formula:

$$\overline{\boldsymbol{r}}(0) = \exp(-\boldsymbol{\Gamma}_\mathrm{b}\overline{d})\ \overline{\boldsymbol{r}}(\overline{d})\ \exp(-\boldsymbol{\Gamma}_\mathrm{f}\overline{d}) \tag{10}$$

In contrast to the analysis with Cartesian coordinates we multiply with different expressions from the left and from the right. For transforming the reflection coefficient at interfaces we can use expressions that were given in [13] for anisotropic material. Therefore, we do not repeat them here. After the input reflection coefficient has been determined, we compute the fields in opposite direction — from the input towards the output. In this way the explicit computation of the exponentially increasing terms can be avoided. The procedure with impedances/admittances is similar.

2.1. Two-dimensional Structures

The derivatives with respect to y are zero in case of two-dimensional structures. Therefore, the polarizations decouple like in the Cartesian case, and we obtain the following operators for the TE- and the TM-polarization:

$$Q_\mathrm{TM} = \begin{bmatrix} -\tan(\theta)\dfrac{\partial}{\partial\overline{v}} & j\left(\mu_\mathrm{r} + \dfrac{\partial}{\partial\overline{v}}\dfrac{1}{\varepsilon_\mathrm{r}}\dfrac{\partial}{\partial\overline{v}}\right) \\ j\varepsilon_\mathrm{r} & -\tan(\theta)\dfrac{\partial}{\partial\overline{v}} \end{bmatrix} \qquad \vec{F} = \begin{pmatrix} E_x \\ \widetilde{H}_y \end{pmatrix}$$

$$Q_\mathrm{TE} = \begin{bmatrix} -\tan(\theta)\dfrac{\partial}{\partial\overline{v}} & -j\mu_\mathrm{r} \\ -j\left(\varepsilon_\mathrm{r} + \dfrac{\partial}{\partial\overline{v}}\dfrac{1}{\mu_\mathrm{r}}\dfrac{\partial}{\partial\overline{v}}\right) & -\tan(\theta)\dfrac{\partial}{\partial\overline{v}} \end{bmatrix} \qquad \vec{F} = \begin{pmatrix} E_y \\ \widetilde{H}_x \end{pmatrix}$$

Instead of working with a coupled differential equation system for the electric and the magnetic field we could also derive a "wave equation" for one field component only. In case of the TE-polarization we obtain e. g., the following expression for E_y:

$$\left[\frac{\partial^2}{\partial\overline{u}^2} + \sin(\theta)\left(\frac{\partial}{\partial\overline{v}} + \mu_\mathrm{r}\frac{\partial}{\partial\overline{v}}\frac{1}{\mu_\mathrm{r}}\right)\frac{\partial}{\partial\overline{u}} + \cos^2(\theta)\mu_\mathrm{r}\varepsilon_\mathrm{r} + \mu_\mathrm{r}\frac{\partial}{\partial\overline{v}}\frac{1}{\mu_\mathrm{r}}\frac{\partial}{\partial\overline{v}}\right] E_y = 0 \tag{11}$$

However, to solve this equation with the MoL, we have to transform it back into a first order differential equation system. Another point should be mentioned: analytically, the wave equation (11) and the coupled equation (7) can be transformed into each other (if we introduce the expression for Q_TE) and are therefore equivalent. On the other hand, a slight difference occurs in discretized form, because of the first order derivatives with respect to v. We will compare those two cases to see the influence on the results.

3. Numerical Results

As first example, we examined the concatenation of a tilted waveguide with a straight input and output waveguide. (see Fig. 2(a)). The diagonal length L was kept constant.

The transmission as function of the angle is shown in Fig. 2(b). Also shown are results that were obtained by a step approximation of the tilted section. To obtain convergent results at least 25 steps were required for $L = 20\,\mu$m with the staircase approximation. In case of $L = 5\,\mu$m this number dropped to 5. When using oblique coordinates the tilted part was examined in one step independent of the length of this section.

Also the two expressions for the oblique coordinates were compared. As can be seen all curves agree very well, the results obtained with the different formulation obained with oblique coordinates are practically indistinguishable.

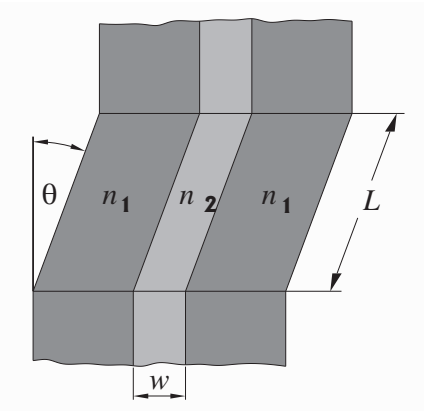

(a)

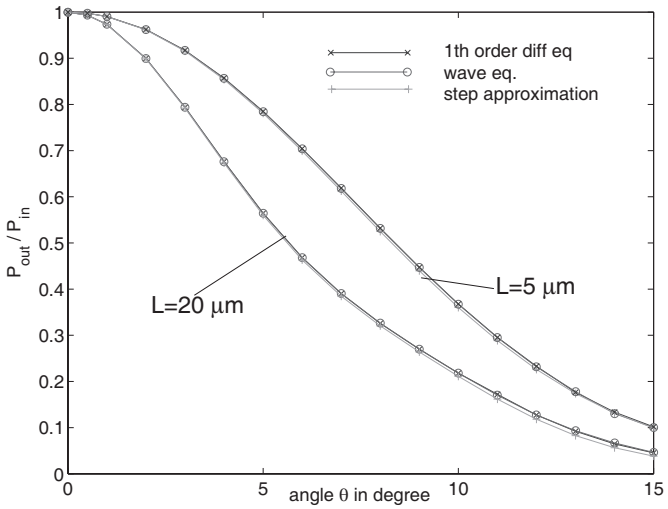

(b)

Figure 2: a) Concatenation of two straight waveguides with a tilted one; data $n_1 = 3.17$, $n_2 = 3.24$, $w = 0.8\,\mu$m, wavelength $\lambda = 1.55\,\mu$m, b) transmission of the fundamental mode.

Next we used oblique coordinates to determine the band structure of photonic crystals with a hexagonal lattice. The structure is shown in Fig. 3. It was taken from [14]. The Floquet modes which must be computed for this band structure were determined with the algorithm presented in [15].

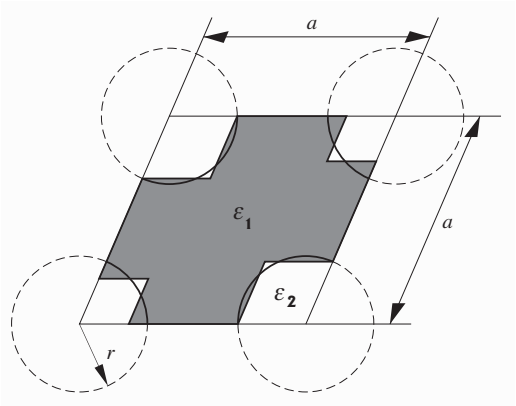

Figure 3: Elementary cell of a hexagonal photonic bandgap structure taken from [14]; data: $r/a = 0.3$, $\varepsilon_1 = 11.56$, $\varepsilon_2 = 1$.

The determined band-structure for the Γ-M band is presented in Fig. 4. Also shown are the values at the

special points Γ and M taken from that reference. A good agreement for the TM-polarization is recognizable, the MoL-curves are slightly higher for the TE-polarization.

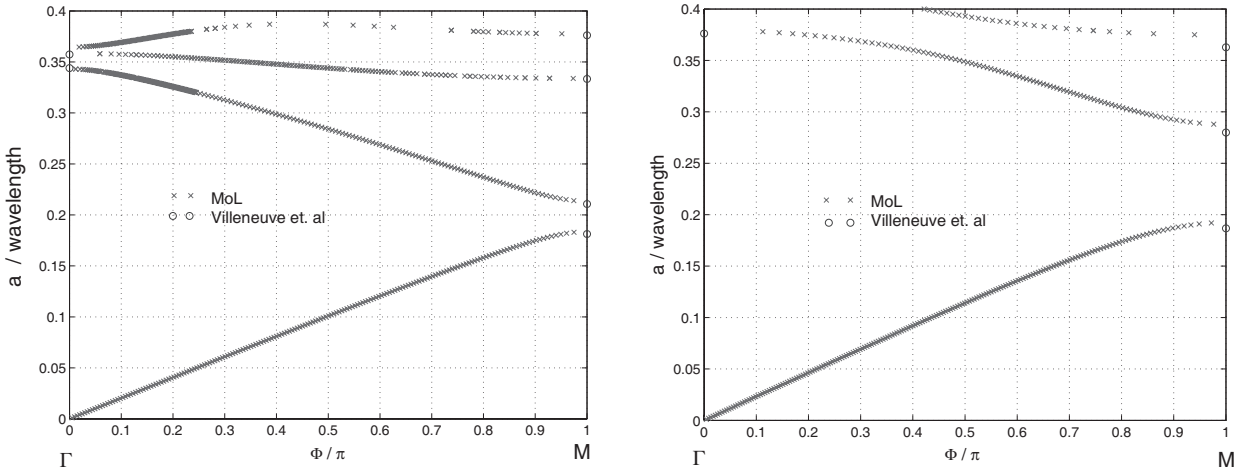

Figure 4: Band structure of a hexagonal lattice a) TM-polarization, b) TE-Polarization.

REFERENCES

1. Pregla, R. and W. Pascher, "The method of lines," *Numerical Techniques for Microwave and Millimeter Wave Passive Structures*, T. Itoh, (Ed.), J. Wiley Publ., New York, USA, 381–446, 1989.
2. Conradi, O., S. Helfert, and R. Pregla, "Comprehensive modeling of vertical-cavity laser-diodes by the method of lines," *IEEE J. Quantum Electron.*, Vol. 37, 928–935, 2001.
3. Pascher, W. and R. Pregla, "Vectorial analysis of bends in optical strip waveguides by the method of lines," *Radio Sci.*, Vol. 28, 1229–1233, 1993.
4. Pregla, R., "The method of lines for the analysis of dielectric waveguides bends," *J. Lightwave Technol.*, Vol. 14, No. 4, 634–639, Apr. 1996.
5. Helfert, S., "Analysis of curved bends in arbitrary optical devices using cylindrical coordinates," *Opt. Quantum Electron.*, Vol. 30, 359–368, 1998.
6. Pregla, R., "Modeling of optical waveguide structures with general anisotropy in arbitrary orthogonal coordinate systems," *IEEE J. of Sel. Topics in Quantum Electronics*, Vol. 8, 1217–1224, Dec. 2002.
7. Helfert, S. F. and R. Pregla, "Efficient analysis of periodic structures," *J. Lightwave Technol.*, Vol. 16, No. 9, 1694–1702, Sep. 1998.
8. Helfert, S. F., "Numerical stable determination of Floquet-modes and the application to the computation of band structures," *Opt. Quantum Electron.*, Vol. 36, 87–107, 2004, Special Issue on Optical Waveguide Theory and Numerical Modelling.
9. Barcz, A., S. Helfert, and R. Pregla, "Modeling of 2D photonic crystals by using the method of lines," *ICTON Conf.*, Warsaw, Poland, Vol. 4, 45–48, 2002.
10. Yamauchi, J., J. Shibayama, and H. Nakano, "Propagating beam analysis based on the implicit finite-difference method using the oblique coordinate system," *OSA Integr. Photo. Resear. Tech. Dig.*, San Francisco, USA, 19–21, Feb. 1994.
11. Benson, T. M., P. Sewell, S. Sujecki, and P. C. Kendall, "Structure related beam propagation," *Opt. Quantum Electron.*, Vol. 31, 689–703, 1999, Special Issue on Optical Waveguide Theory and Numerical Modelling.
12. Sewell, P., T. M. Benson, S. Sujecki, and P. C. Kendall, "The dispersion characteristics of oblique coordinate beam propagation algorithms," *J. Lightwave Technol.*, Vol. 17, No. 3, 514–518, 1999.
13. Helfert, S. F. and R. Pregla, "The method of lines: a versatile tool for the analysis of waveguide structures," *Electromagnetics*, Vol. 22, 615–637, 2002, Invited paper for the special issue on "Optical wave propagation in guiding structures".

14. Villeneuve, P. R., S. Fan, S. G. Johnson, and J. D. Joannopoulos, "Three-dimensional photon confinement in photonic crystals of low-dimensional periodicity," *IEE Proc.-Optoelectron.*, Vol. 145, No. 6, 384–390, 1998.
15. Helfert, S. F., "Determination of Floquet-modes in asymmetric periodic structures," *Opt. Quantum Electron.*, Vol. 37, 185–197, 2005, Special Issue on Optical Waveguide Theory and Numerical Modelling.

Mixed-mode Optical Design for Optoelectronic Applications

N. Danz, **D. Michaelis**, **P. Schreiber**, **C. Wähter**, **and U.-D. Zeitner**
Fraunhofer Institute for Applied Optics and Precision Engineering, Germany

This paper aims to highlight the variability of tools and methods which are required for the optical design of optoelectronic systems, which may include sources, receivers, refractive and diffractive micro-optical elements as well as waveguides and photonic crystals.

What details of the character of the electromagnetic field in a design are to be considered strongly depends on the systems geometry. High refractive indices and geometry features at wavelength scale or below require vectorial analysis, whereas low index contrast, small numerical aperture (NA) and field diameters well above the wavelength may allow for simple ray optics. If the optical system includes quite different media and different length-scales, due consideration is needed in order to determine a possible design flow which is both sufficiently accurate and numerically feasible. If approximations are unavoidable, the cross-check of the results with complementary methods is a must in order to achieve reliability of the design prior to fabrication. Thus, a variety of different design tools has to be at hand within the design process, for e.g., fibre to photonic crystal coupling, diffractive correction, and light extraction from OLED devices, for example.

If the coupling from a telecom fibre to a defect waveguide in a photonic crystal by means of free-space micro-optics is considered, it is intuitively clear that FDTD isn't applicable for the whole geometry, whereas considerable parts of the system are best handled with ray-tracing, simply. In order to improve design efficiency, a semi-analytical model to calculate the transmission from the focal field (foc) to the intended waveguide mode (w) as an integral over a coupling plane (cp)

$$T = \frac{\left| \iint\limits_{(cp)} dxdy \left[\vec{E}_{Foc}^{(t)^*} \times \vec{H}_{W}^{(t)} + \vec{E}_{W}^{(t)} \times \vec{H}_{Foc}^{t^*} \right]_z \right|^2 - \left| \iint\limits_{(cp)} dxdy \left[\vec{E}_{Foc}^{(t)} \times \vec{H}_{W}^{(t)} - \vec{E}_{W}^{(t)} \times \vec{H}_{Foc}^{t} \right]_z \right|^2}{\iint_{(cp)} dxdy \left[\vec{E}_{Foc}^{(t)^*} \times \vec{H}_{W}^{(t)} + \vec{E}_{W}^{(t)} \times \vec{H}_{Foc}^{(t)^*} \right]_z}$$

can be used advantageously [1], which is based on the reciprocity theorem for photonic crystal waveguides [2]. To confirm the result, FDTD is a proper means now since the volume required for the analysis just allows for a discretisation which fits into a PCs memory.

Diffractive elements in micro-optical systems call for separate investigation. Scalar diffraction theory turns out to be a simplified approximation if e.g. diffractive corrections are applied to high NA micro-lenses. In order to incorporate efficiencies and phases for different diffraction orders accurately in an overall design, rigorously coupled wave analysis applied to grating problems is an adequate means. The coupling of grating analysis and a ray-trace engine is a must, too, if light extraction from OLEDs by means of periodic structures is investigated. Furthermore, for the OLED device the coupling of light from the radiating dipoles into slab guided and leaky modes requires special consideration, since this may reduce the overall device efficiency remarkably. There, a Green-functions based analysis tool is an adequate means for design improvements.

Although commercially available design tools nowadays offer a wide range of functionality, these examples which all stem from applied research show that the diversity of optical applications requires that the designer can fall back to different design tools, to appropriate interface tools, and to a sufficiently broad knowledge in electromagnetics.

REFERENCES

1. Michaelis, D., et al., "Coupling coefficients of photonic crystal waveguides," SPIE, Vol. 4987, 114–125, 2003.
2. Michaelis, D., et al., "Reciprocity theorem and perturbation theory for photonic crystal waveguide," *Phys. Rev. E* , Vol. 68, 065601(R), 2003.

Modelling of Time-varying Phenomena in Electroabsorption Modulators

A. Vukovic, **E. Bekker**, **P. Sewell**, **and T. M. Benson**
The University of Nottingham, UK

Modern RF electroabsorption modulators are important devices as they directly determine the bandwidth, speed and operational frequency of dense wavelength division multiplexing (DWDM) and optical time division multiplexing systems (OTDM). In these systems they are commonly used for short pulse generation, data encoding and clock recovery. In order to enable systems achieve higher speed, bandwidths and lower costs an efficient modelling tool that would enable deeper insight into the physical behaviour of the modulator and its existing problems and limitations is needed.

The principal operation of a RF electroabsorption modulator relies on the interaction of the optical electromagnetic wave with the time-varying medium whose complex dielectric constant is modulated by a microwave wave. The optical wave is confined by a complex semiconductor geometry and the modulation of the dielectric constant is done in a relatively small region of a multiple quantum well (MQW). It is well known that a temporal change of the dielectric permittivity in an open and semi-open medium causes transformation of the original plane wave into reflected and transmitted waves of different frequencies and same wave numbers [1, 2]. In the time-varying waveguide the change of the permittivity directly affects not only the frequency of the incident wave but also the spatial distribution of the wave which further complicates the problem.

One of the major limitations in the performance of RF modulators is the temporal variation of the frequency and this is measured through the chirp parameter.

Numerical methods such as the Finite Difference Time Domain (FDTD) and the Transmission Line Modelling (TLM) method can in general be used to model time-varying phenomena but they do not allow for the physical investigation of the problem. On the other hand exact analytical methods have been confined to a few special cases of infinite and semi-infinite media [1, 2] and slab waveguides [3].

This paper investigates a semi-analytical Time Domain Spectral Index (TDSI) technique [4] that enables efficient modelling of propagation of the optical signal through a time-varying rib waveguide and is suitable for predicting the chirp parameter. For the complex case of a time-varying dielectric waveguide, invariant in the z-direction, the solution of the wave equation yields waves (incident and reflected) having new frequencies and preserved wavenumbers. The new spatial wave distribution of the secondary waves is obtained by reversing the original spectral wave problem of the TDSI and solving for a new frequency. The amplitudes of all incident and reflected waves are solved using the Galerkin approach with triangular and Gaussian basis functions. The method is verified for cases of temporal dielectric change in an open region and a slab waveguide and then extended to include an air-clad waveguide. The method is applied to model the chirp parameter in a typical electroabsorption waveguide.

REFERENCES

1. Morgenthaler, F., "Velocity modulation of electromagnetic waves," *IRE Trans. On Microwave Theory and Technique*, 167–172, 1958.
2. Fante, R., "Transmission of electromagnetic waves into time-varying media," *IEEE Trans ons Antennas and Propagation*, Vol. AP-19, No. 3, 417–424, 1971.
3. Nerukh, A., P. Sewell, and T. M. Benson, "Volterra integral equations for nonstationary electromagnetic processes in time-varying dielectric waveguides," *J. of Lightwave Techn.*, Vol. 22, No. 5, 1408, 2004.
4. Bekker, E., A. Vukovic, P. Sewell, and T. M. Benson, "A novel hybrid approach for modelling of electroabsorption modulators," 7^{th} *International Conference on Transparent Optical Networks ICTON*, 147–151, 2005.

High-Q Photonic Crystal Microcavities in Diamond

S. Tomljenovic-Hanic[1], M. J. Steel[2,1], and C. M. de Sterke[1]

[1]University of Sydney, Australia
[2]RSoft Design Group, Inc., Australia

There has recently been great interest in optical microcavities based on photonic crystal slabs (PCS) [1–3]. Almost all of these studies consider a two-dimensional PCS composed of a hexagonal array of cylindrical air holes in a silicon dielectric slab ($n \approx 3.4$). In this study, the material chosen is diamond ($n \approx 2.4$) because of its unique possibilities for demonstrating quantum entanglement of N-V centres. The photonic crystal geometry is potentially advantageous in achieving entanglement, since it can enable strong confinement in cavities and optical coupling between different centres [4].

The quality factors of defects in PC slabs are strongly influenced by the position and widths of the photonic band gaps (PBG). Consequently, the first step is to design an infinite periodic structure without a cavity. Subsequently, the finite structure including the cavity defect can be optimized to obtain the highest quality factor possible. We find that the PBG widths of diamond PCS are comparable with silicon-based PCS whereas the positions of corresponding gaps differ. Consequently the in-plane quality factors for the two materials are similar, whereas the out-of-plane factor for diamond is smaller.

The optimization of optical cavity design, i.e., further tuning of the quality factor is possible by modifying the geometry of the lattice structure surrounding the cavity. For example Noda et al. constructed a cavity by three missing air holes in a row of a silicon slab with hexagonal lattice structure [1, 2]. They optimized the structure by shifting the left and right air holes outwards. We apply a similar method to the diamond based structure and find that high-Q microcavities can be designed in this material.

*This work was produced with the assistance of the Australian Research Council (ARC) under the ARC Centres of Excellence Program. CUDOS (the Centre for Ultrahigh-bandwidth Devices for Optical Systems) is an ARC Centre of Excellence.

REFERENCES

1. Akahane, Y., T. Asano, B. S. Song, and S. Noda, *Nature*, Vol. 425, 944, 2003.
2. Akahane, Y., T. Asano, B. S. Song, and S. Noda, *Opt. Express*, Vol. 13, 1202, 2005.
3. Srinivasan, K. and O. Painter, *Opt. Express*, Vol. 11, 579, 2003.
4. Salzman, J., S. Prawer, and D. Jamieson, *Photonic Crystal Devices and Systems in Diamond*, Provisional Patent, CCID 131000480.

Nonlinear Pulse Propagation and Modulation Instability in Periodic Media with and without Defects

V. Grimalsky[1], **S. Koshevaya**[2], **J. Sanchez-Mondragon**[1]
M. Tecpoyotl-Torres[2], **and J. Escobedo-Alatorre**[2]
[1]National Institute for Astrophysics, Optics, and Electronics (INAOE), Mexico
[2]Autonomous University of Morelos (UAEM), Mexico

Abstract—The nonlinear propagation of EMW in periodic media is of great interest due to the possibility to accumulate energy in periodic media within the stop band and, therefore, the input intensity levels for observation of nonlinear phenomena are quite low [1]. For resonant interactions, also it is possible to realize matching conditions, which are not possible in uniform media. Both resonant multiwave interactions and self-action of EMW in nonlinear periodic media have been analyzed [1, 2]. Also, a method based on a slow variation in time was proposed, which seems more adequate than others based on coupled equations [3].

The presence of defects in periodic structure leads to narrow regions of transmission within the stop-band. In this case, the application of coupled equations for counter propagating waves becomes doubtful, and a more general approach is needed [3]. Also, the influence of defects on the dynamics of modulation instability of long pulses is of a great interest. The present paper considers numerical simulations of the pointed above phenomena. For a correct description of the nonlinear dynamics, it is necessary also to take into account the wave dissipation and possible transverse diffraction.

The results of simulations demonstrated the essential influence of defects within the periodic structure on the nonlinear propagation of EM pulses, even if the carrier frequency is chosen within the stop band of the structure with a defect. This fact can be explained by a quite wide spectrum of the input pulse, and the "tail" of such a spectrum is within the transmission region due to the defect. This situation is analogous to the nonlinear propagation of short spin-dipole waves in the vicinity of the cut-off frequency [4]. The dynamics of modulation instability also changes in the presence of the defect. The diffraction can affect essentially the modulation instability dynamics.

1. Basic Equations

The case under research is the nonlinear periodic medium (OABAB...O), where A and B are dielectrics, and O is the vacuum. Each layer is assumed as isotropic and the influence of temporal dispersion is neglected here. The last consideration is valid only if the duration of the input pulse is long (> 0.1 ps). Within the structure, the presence of a singe defect is possible (such as ...ABABBBAB...). Consider almost transversely polarized EM wave, where only a single transverse component of the electric field (for instance, E_x) is dominating. A weak dependence on the radial coordinate is taken into account, to estimate an influence of diffraction. We use a slow dependence of the wave amplitude A only respect to time (essentially its variation in space, due to periodic structure of the medium), cubic non linearity and step-like dependence of the dielectric permittivity. Different spatial harmonics (both co- and counter-propagating) are included into the wave structure within the periodic lattice:

$$\frac{\partial A}{\partial t} + \frac{i\omega}{2}\left(1 + \frac{\Delta\varepsilon}{\varepsilon(z)}\right)A + \frac{i}{2\omega\varepsilon(z)}\left(\frac{\partial^2 A}{\partial t^2} + \nabla_\perp^2 A\right) + \gamma A = 0; \quad \Delta\varepsilon = \alpha(z)|A|^2 \tag{1}$$

Here $\Delta\varepsilon(E)$ is the change on the dielectric permittivity of the periodic medium due to the cubic nonlinearity. The scale of longitudinal spatial dependence is arbitrary, because of step-like dependence of dielectric permittivity. Then, the electric field is considered as:

$$E = \frac{1}{2}A(z, \rho, t) \times \exp(i\omega t) + c.c. \tag{2}$$

In equation (1), $\varepsilon = \varepsilon(z)$ is the dielectric permittivity of the periodic medium, ω is the carrier frequency ($\omega = 2\pi c/\lambda_0$, with λ_0 the wavelength in vacuum). Also the wave dissipation γ is included in this equation.

The boundary conditions at the interfaces between the layers are taken into account in Equation (1). Additionally, it is necessary to consider the boundary conditions for the tangential components of electric and magnetic fields at the input ($z = 0$) and at the output ($z = L$) of the periodic medium:

$$z = 0: \quad A = A_{inc} + A_{refl}; \quad \frac{\partial A}{\partial z} \approx \frac{\partial A_{inc}}{\partial z} + \frac{\partial A_{refl}}{\partial z} \tag{3a}$$

where: $A_{inc}(z,\rho,t) \approx A_{i0}(\rho,t)\times\exp(-ik_0 z)$; $A_{refl}(z,\rho,t) \approx A_{r0}(\rho,t)\times\exp(+ik_0 z)$, A_{i0}, A_{r0} are the amplitudes of incident and reflected waves, respectively; $k_0 = \omega/c$ is the wave number of the wave in vacuum. It is assumed that the amplitude of the incident wave is known.

Equation (3a) can be reduced as it is shown in the following boundary conditions:

$$z = 0: \quad \frac{\partial A}{\partial z} - ik_0 A \approx -2ik_0 A_{i0}(\rho,t) \qquad z = L: \quad \frac{\partial A}{\partial z} + ik_0 A \approx 0. \tag{3b}$$

Equation (1) and boundary conditions (3) are valid in the case of transversely wide pulses. Otherwise, it is impossible to use the approximation of transversely polarized EM wave.

2. Method of Simulations

The splitting with respect to physical factors is applied. The problem of stability of simulations is very important because the possible modulation instability is under research. The full explicit three-layer scheme is used for nonlinearity, dissipation, and longitudinal transport fractional step. Two-layer implicit scheme is utilized for the diffraction fractional step. In simulations, the one-dimensional representation of Equation (1) has been used:

$$\frac{\partial \bar{A}}{\partial \bar{t}} + \frac{i\bar{\omega}}{2}\left(1 + \frac{\Delta\varepsilon}{\varepsilon(\bar{z})}\right)\bar{A} + \frac{i}{2\bar{\omega}\varepsilon(\bar{z})}\left(\frac{\partial^2 \bar{A}}{\partial \bar{z}^2} + \frac{1}{\bar{\rho}}\frac{\partial}{\partial\bar{\rho}}\left(\bar{\rho}\frac{\partial \bar{A}}{\partial\bar{\rho}}\right)\right) + \bar{\gamma}\bar{A} = 0; \quad \Delta\varepsilon = b(\bar{z})|\bar{A}|^2 \tag{4}$$

where $\bar{z} = z/l_n$, $\bar{t} = t/t_n$, $t_n = l_n/c$; $\bar{\rho} = \rho/l_n$.

The value of $l_n = 1\,\mu$m has been chosen; thus, $t_n = 3.15\times10^{-15}$ s. Below, the lines over the one-dimensioned quantities (t, z, ρ, A) are omitted, because we use one-dimensional representation. The shape of the input pulse is:

$$A_i(t,\rho) = A_{i0}\times\exp\left(-\left(\frac{t-t_1}{t_0}\right)^4\right)\times\exp\left(-\left(\frac{\rho}{\rho_0}\right)^4\right) \tag{5}$$

3. Results of Simulations

The structures under simulation include 48 layers, their dielectric permittivities are $\varepsilon_A = 3.5$, $\varepsilon_B = 2.0$. A-layers are nonlinear ($b = -0.1$), whereas B-layers are assumed as linear ($b = 0$). Each layer has a length of $0.25\,\mu$m. A single defect is replacement of the 23^{rd} A-layer by a B-layer. The central frequency has been chosen in the region of the stop-band. In Fig. 1, the linear transmission coefficients are given for the cases of the

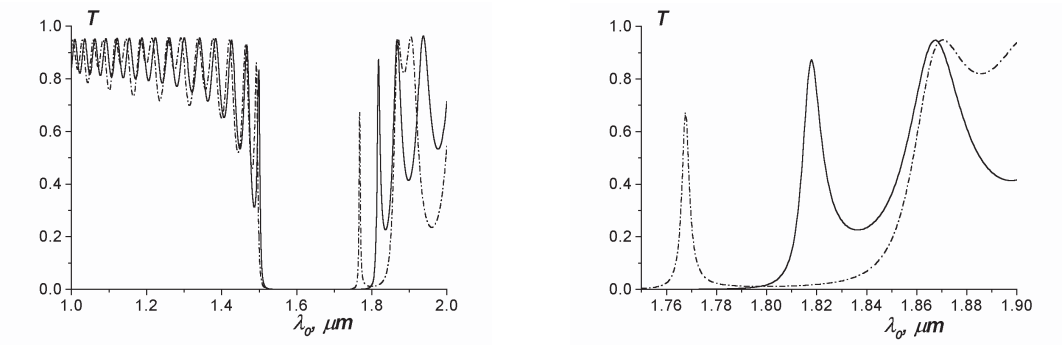

(a) (b)

Figure 1: Linear transmission coefficients. a) The general picture, b) A section only. Note that the solid lines correspond to the case without defect and the dotted line is for with defect.

periodic structure without and with the single defect. The presence of the single defect causes a narrow region of transparency and a shift of the limits of the stop-band. Therefore, the most interesting regions of the central wave numbers (or frequencies) are localized near the upper limit of wave numbers ($\lambda_0 \sim 1.80\,\mu$m). Note that in the linear case the total reflection takes place for the monochromatic input EM wave.

In Fig. 2, the nonlinear transmission coefficients of monochromatic waves are given in the structures with and without defect. In the structure with defect the transmission coefficient gets more broken dependence, in comparison with the linear case. More over, in the vicinity of the narrow transmission region, the shape of such dependence becomes chaotic-like. This fact can be explained by the accumulation of the energy of EM oscillations at the defect of the lattice.

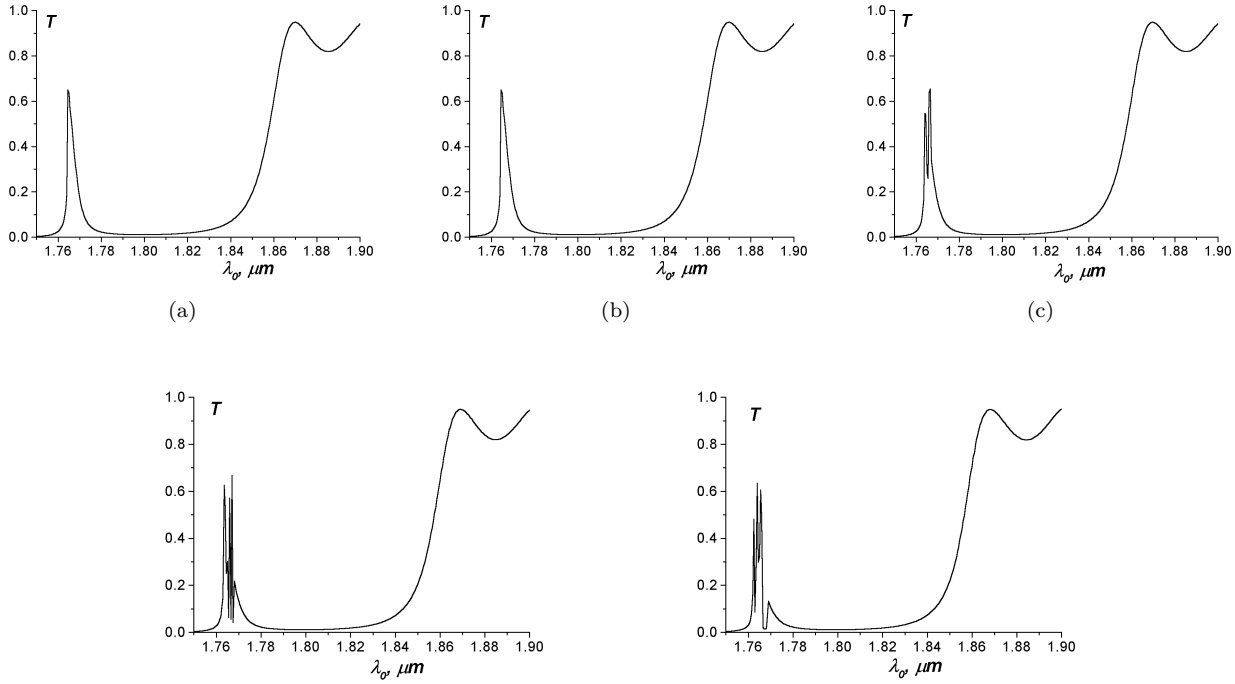

Figure 2: Nonlinear transmission coefficients through the structure with the defect for the monochromatic wave: a) with $A_0 = 0.01$ (linear case), a) $A_0 = 0.1$, b) $A_0 = 0.12$, c) $A_0 = 0.15$, d) $A_0 = 0.2$. For a comparison, e) is for $A_0 = 0.2$ (the regular structure).

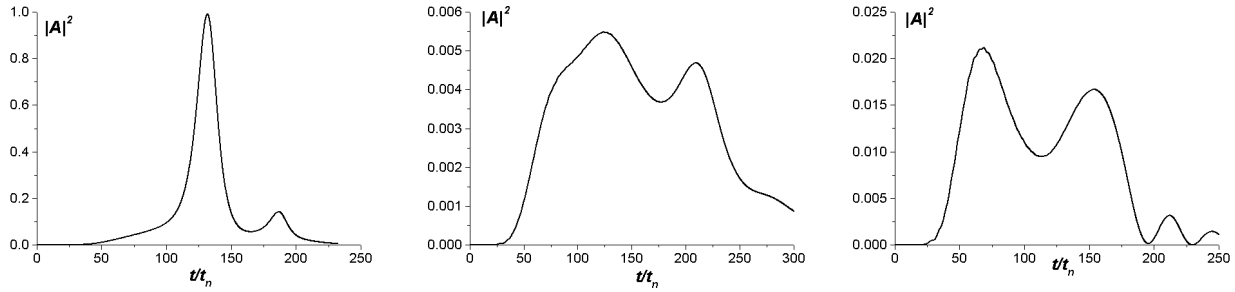

Figure 3: Propagation of the short transversely wide pulses. The carrier frequency corresponds to the wave number $\lambda_0 = 1.80\,\mu$m. Part a) is the nonlinear propagation though the regular structure ($A_0 = 1$); b) the same as a), but the input amplitude is 3 times smaller ($A_0 = 0.31$); c) the same input pulse as a) ($A_0 = 1$) but the propagation through the structure with defect.

Two different situations can occur due to the dependence on the duration of the incident pulse. The first one corresponds to relatively short pulses. The typical results of simulations are given in Figs. 3 and 4. Here the intensities of transmitted pulses are presented in the figure captions; $t_1 = 100$, $t_0 = 80$. In the case of the regular periodic structure, the nonlinear transparency phenomenon occurs at lower amplitudes of the input pulse, compare Fig. 3(a) and 3(c). In the case of the structure with the defect, the amplitude of the transmitted pulse is quite small even in nonlinear case, Fig. 3(c). The simulations of nonlinear propagation of transversely narrower pulses have demonstrated that an influence of diffraction is not expressed for the maximum of the transmitted pulse but changes weakly the rear part of it.

A comparison of Figs. 3 and 4 has demonstrated that a relatively small shift of the central frequency of the pulse changes the nonlinear dynamics essentially. Moreover, the regular periodic structures and ones with the

defect possess different frequency regions for the manifestation of the nonlinear transparency phenomenon.

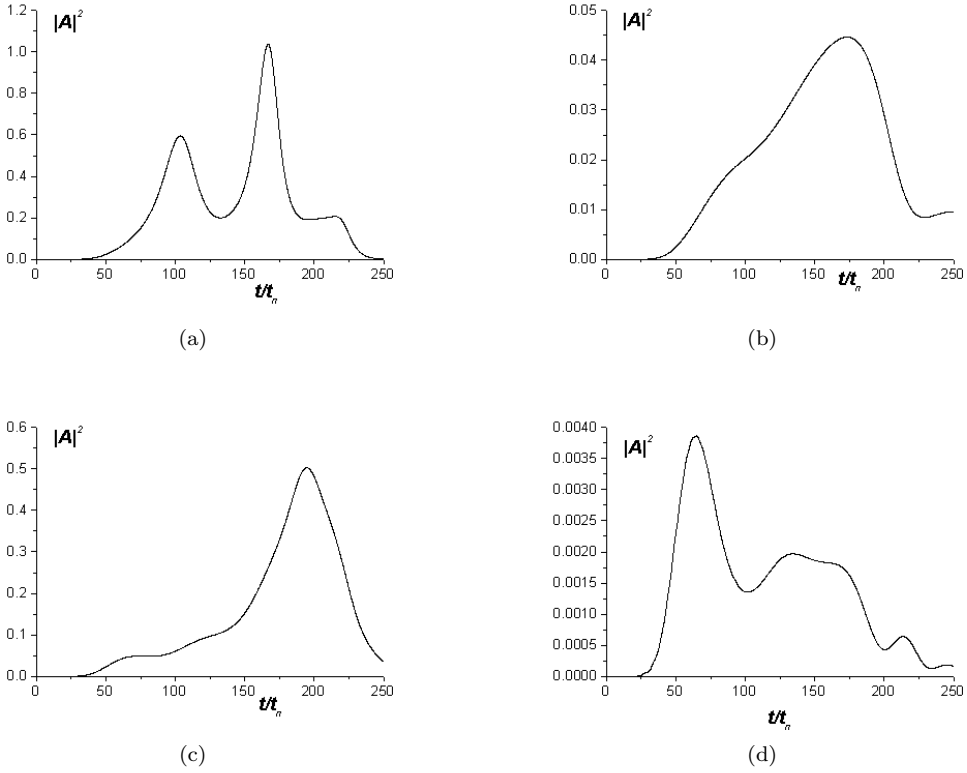

Figure 4: Propagation of the short, transversely wide pulses. The carrier frequency corresponds to the wave number $\lambda_0 = 1.82\,\mu$m. Part a) is the nonlinear propagation though the regular structure ($A_0 = 1$); b) the same as a), but the input amplitude is 3 times smaller ($A_0 = 0.31$); c) and d) are the same input pulses as a) and b) ($A_0 = 1$, $A_0 = 0.31$) but the propagation is through the structure with defect.

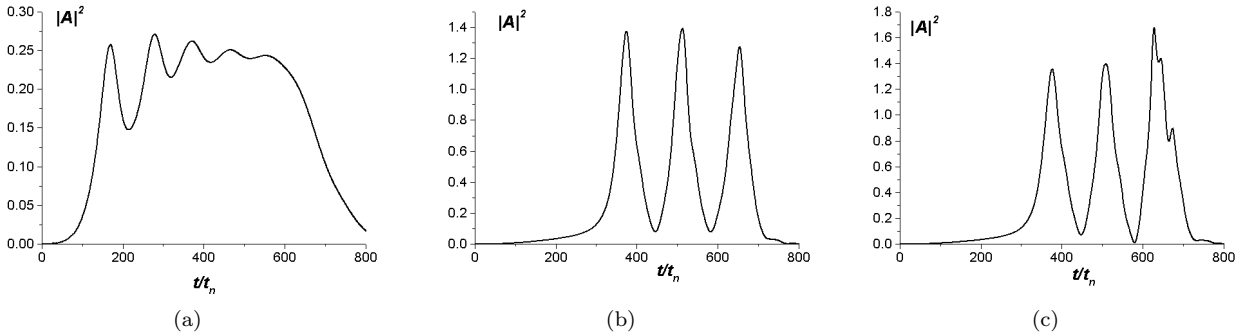

Figure 5: Modulation instability with and without defects. The carrier frequency corresponds to the wave number $\lambda_0 = 1.82\,\mu$m. The maximal input amplitude is $A_0 = 1.00$. Part a) is for the regular structure, b) is for the structure with defect ($\rho_0 = 60$), c) is for the structure with defect (with an influence of diffraction, $\rho_0 = 24$).

The case of much longer incident pulses corresponds to the occurrence of modulation instability (MI). Here the general picture is somewhat different from the previous case, see Figs. 5 and 6. The parameters of the input pulses are $t_0 = 340$, $t_1 = 400$. At the output of the structure the multipeak signal occurs. Also, the role of diffraction is essentially expressed; compare Fig. 6(d) and 6(e). In the case of MI developed, the influence of

temporal dispersion can be essential, and the used approximation cases its validity.

An interesting result of simulations is also the fact that the regular structure and one with the defect possess different frequency regions of observing modulation instability within the stop-band.

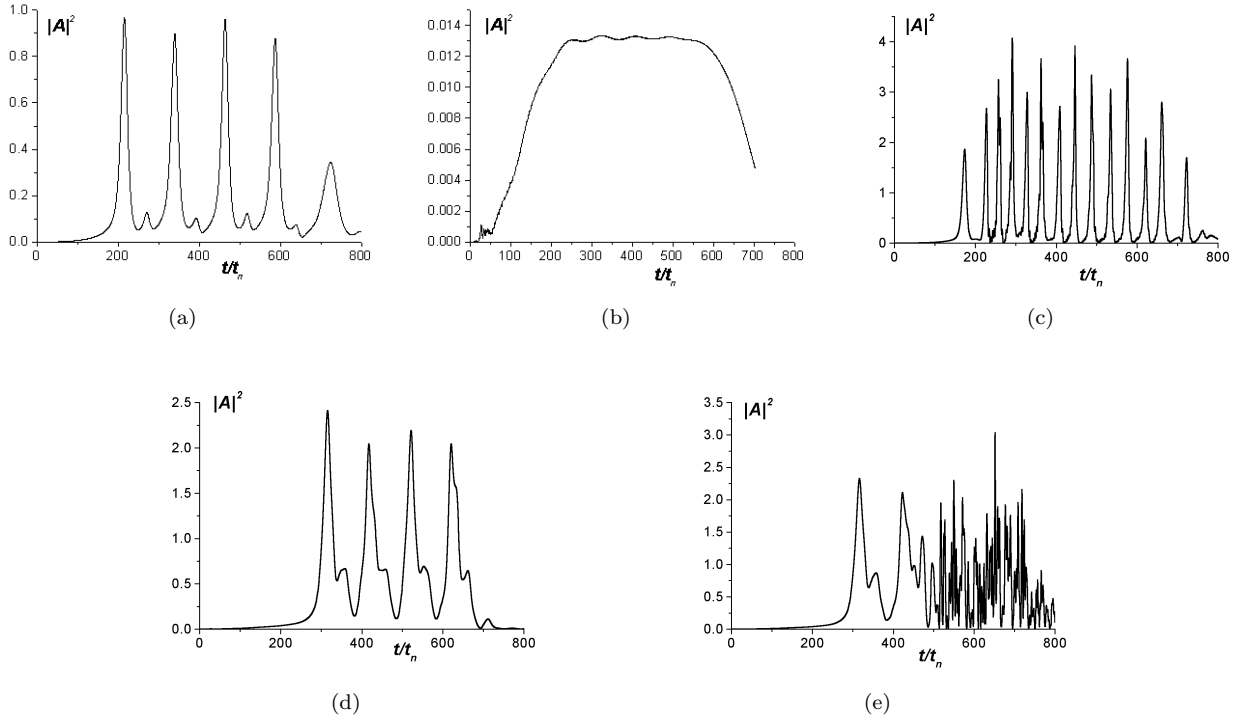

Figure 6: Modulation instability with and without defects. The carrier frequency corresponds to the wave number $\lambda_0 = 1.80\,\mu$m. Part a) is for the regular structure, $A_0 = 1.0$, (transversely wide pulse, $\rho_0 = 60$); b) is for the structure with defect, $A_0 = 1.0$ ($\rho_0 = 60$); c) is for the regular structure, $A_0 = 1.41$ ($\rho_0 = 60$); d) is for the structure with defect, $A_0 = 1.41$ ($\rho_0 = 60$); e) is for the structure with defect, $A_0 = 1.41$ (transversely narrow pulse, $\rho_0 = 24$).

4. Conclusions

The results of simulations have been demonstrated an essential influence of defects within the periodic structure on the nonlinear propagation of EM pulses, even if the carrier frequency is chosen within the stop band of the structure with the defect. This can be explained by a quite wide spectrum of the input pulse, and the "tail" of such a spectrum is within the transmission region due to the defect. The dynamics of modulation instability also changes in the presence of the defect. The diffraction can affect essentially the modulation instability dynamics.

Acknowledgment

This work was partially supported by CONACyT (Mexico) under grant 45667-F.

REFERENCES

1. Gupta, S. D., "Nonlinear optics of stratified media," *Progress in Optics*, Elsevier, Amsterdam, NL, Vol. 38, 3–84, 1998.
2. Escobedo-Alatorre, J., J. Sanchez-Mondragon, M. Torres-Cisneros, R. Selvas-Aguilar, and M. Basurto-Pensado, "A device approach to propagation in nonlinear photonic crystal," *Optical Materials*, Vol. 27, No. 7, 1260–1265, 2005.
3. Scalora, M. and M. E. Crenshaw, "A beam propagation method that handles reflections," *Opt. Commun.*, Vol. 108, 191–196, 1994.
4. Burlak, G., V. Grimalsky, S. Koshevaya, and P. Marquez-A, "Dynamics of magnetostatic wave solitons in the vicinity of frequency cut-off," *Journ. of Magn. Magn. Mater.*, Vol. 237, No. 1, 97–103, 2001.

Nonlinear Vector Finite Element Simulation of Optical Photonic Devices

A. Fisher[1], **D. White**[2], **and G. Rodrigue**[1]

[1]University of California, USA
[2]Lawrence Livermore National Laboratory, USA

Continual research of new optical devices for use in the communication industry has led to the possibility of using the nonlinear optical response of various materials. Using these nonlinear effects, researchers have been designing switches, logic gates, and frequency generators with increasing complexity in both functioning and geometry. The high degree of complexity in functioning makes analysis of these devices through analytical approximation incomplete. Significant progress in understanding these devices has been made through the use of simulation using nonlinear Finite Difference Time Domain (FDTD) schemes. While the FDTD schemes are highly computationally efficient, the increasing geometric complexity of these devices is becoming a problem for the FDTD approach given its highly restrictive geometry constraints.

We present a nonlinear Vector Finite Element Method (VFEM) scheme that involves discretizing Maxwell's equations using Nedelec edge and face bases. The VFEM scheme is capable of simulating instantaneous third order nonlinear processes such as the the kerr effect, and four wave mixing. The VFEM scheme is also capable of handling the complicated 3 D geometries found in many of the newer optical photonic devices with a high degree of accuracy. Also, our VFEM scheme includes methods for reducing the high computational cost of nonlinear finite element methods, thereby making larger simulations possible.

In addition to presenting this new scheme, we will also present a series of tests to show that the scheme is capable of simulating the intricacies of optical photonic devices. These tests include simulations of classical nonlinear optical effects that can be compared with analytical approximations. The tests also include some comparisons to FDTD schemes on less complicated geometries. Finally, with a reasonable degree of confidence in the accuracy of the scheme, we will present novel simulations of some optical photonic devices.

Modelling of Bragg Gratings and Application in Cascaded Cavities

A. Melloni, F. Morichetti, and M. Martinelli
Politecnico di Milano, Italy

Nowadays advanced electromagnetic numerical methods and powerful computing availability allow the analysis of most of the optical structures and devices with a great accuracy. These methods (FDTD, FEM, ...) can be extremely accurate but often they are extremely time and memory consuming, especially if 3D structures are considered. Whilst an electromagnetic approach is undoubtedly convenient for the analysis of the linear behavior, for the non-linear analysis, synthesis and optimizations of more complex devices they are often of poor utility.

In this contribution we explain how an accurate modelling of a simple building block, like the Bragg reflector, can be of great aid in both linear and nonlinear analysis of complex circuits, such as cascaded coupled cavities. The concept of using an equivalent circuit instead of a more physical description of the device is well grounded in both electronic and microwave domain and can be applied advantageously also in the optical field.

A possible equivalent circuit of the Bragg grating shown in Figure 1(a) is composed by an ideal partially reflecting mirror (r, t, φ_0) placed between two sections of propagating regions (L_e, n_0), as shown in Figure 1(b). The reflectivity r and the equivalent length L_e can be determined analytically, numerically or experimentally [1].

In the nonlinear domain the equivalent circuit can powerfully maintain its validity, provided that the nonlinear coefficient of the two sections L_e is given by $n_{2e} = n_2 L_p / 2L_e$ where n_2 is the nonlinear refractive index of the material and L_p is the effective nonlinear length, defined as the distance over which the nonlinearity really acts. By integrating the electric field over the physical length of the grating, it is found that the nonlinear length is equal to the penetration depth $L_p = tanh(kL)/kL$, that is the group length (k being the grating coupling coefficient). To show the potentialities of such an approach, let's consider two cascaded cavities defined by three gratings (detailed data of the structure can be found in [2]). The spectral behavior in the linear regime of the whole structure is the bell-shaped response centered at 1.55 μm shown in Figure 2. As the input power increases, the spectral response shifts toward the right and deforms under the effect of the Kerr nonlinearity. For high power levels, a bistability region appears on the right side of the response, close to the band-edge. The nonlinear response, both in frequency and time domain, can be computed very efficiently and a comparison with results obtained with electromagnetic simulators show a very good agreement.

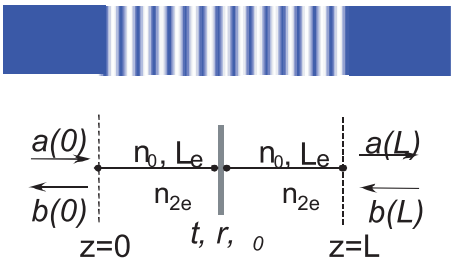

Figure 1: a) Generic bragg grating; b) its linear and nonlinear equivalent circuit.

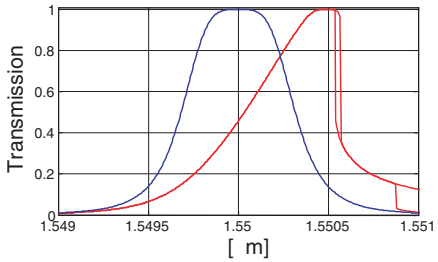

Figure 2: Spectral transfer function of two cascaded cavities in linear and nonlinear regime.

REFERENCES

1. Melloni, A., et al., "Equivalent circuit of bragg gratings and its application to fabry-perot cavities," *JOSA A*, Vol. 20, No. 2, 273–281, 2003.
2. *Slow-wave Task of the European COST Action P11–WG2*, http://w3.uniroma1.it/energetica/

Spectral-element Discontinuous Galerkin (SEDG) Simulations for Metallic Nanoparticles

M. Min and P. F. Fischer
Mathematics and Computer Science Division, USA

We present higher-order computational methods to study the dynamic nature of electromagnetic waves interacting with metallic nanoparticles where strong surface plasmon excitations can occur. In the study of light interacting with a nanoscale object, a particular computational issue is that the problem includes sharp discontinuities in the dielectric function along the surface of the nanoscale object. In such cases, standard lower-order methods such as FDTD method require considerable computational work in order to achieve a certain expected accuracy. The drawback comes from the slow rate of convergence of the methods for problems whose solutions have less regularity in smoothness. We propose to use higher-order numerical techniques with phase-preserving nature: a spectral-element discontinuous Galerkin (SEDG) method. The method is based on multidomain body-conforming approach. The exponential accuracy of this method without stair-stepping phenomena will be discussed. Computational performance of 3D structures and simulation for metallic nanosphere waveguide will be demonstrated.